scientific reports

Check for updates

OPEN

Effects of antihypertensives on the degradation behavior of AZ31 alloy in in-vitro environment

Gang Xiao[1], Min Fan[2]✉, Kui Wang[3,4,5]✉, Haonan Li[3], Yazhao Shen[3], Xufeng Cai[3], Haiyan Jiang[3], Guangling Wei[3]✉ & Haiyan Yang[6]

Effects of seven antihypertensives of *Losartan Kalicum*(LK), *Atenolol*(ATEN), *Nifedipine*(NF), *Hydrochlorothiazide*(HCTZ), *Valsartan*(VLA), *Furosemide*(FUR) and *Captopril*(CAP) have been investigated on the degradation behavior of AZ31 alloy in simulated body fluid (Hank's solution). LK, NF and HCTZ with the concentrations of 0.5, 1.0 and 0.5 g/L can remarkably enhance the degradation resistance of AZ31 alloy by 63.1, 69.4 and 70.5%, respectively. The surface analysis reveals that the addition of LK, NF and HCTZ can reduce degradation rate by promoting the growth of hydroxyapatite, increasing the protection effect of corrosion film formed. The present results may enhance the corrosion resistance of Mg-based orthopedic implants.

Keywords Antihypertensives, AZ31 alloy, Degradation rate, Hydroxyapatite, Corrosion film

In the past few decades, metallic implants have attracted much attention and been widely applied in the orthopedic repair issues[1,2]. Compared with the traditional implant materials such as stainless steels and titanium-based alloys[3–5], the desirable similarity of density, Young's modulus and mechanical properties to human bones, which can minimize the "stress shielding" effect[6] caused by the traditional ones, makes the magnesium alloys a more promising material in the orthopedic application[7–12]. More importantly, Mg ions with the consumption of 250 ~ 300 mg/day are the daily common metabolite in human bodies[13,14]. The extra Mg ions generated by the degradation of magnesium implants can be excreted from the body in the form of urine[15], and thus the complications can be effectively avoided in this way. At present, the magnesium alloys commonly used as the biomaterials mainly include pure Mg, AZ31, AZ91, WE43 and Mg-Ca alloys[16–20]. Although magnesium alloy implants have many advantages, the high degradation rate still limits their wide application in the physiological environments. The excessive hydrogen released during the degradation may lead to a reduction in the mechanical strength and stability of magnesium implants[21–23], compromising the rehabilitation of injured bones. Thus, the enhancement of the corrosion resistance of magnesium alloy implants is of great necessity to satisfy the clinic requirements and biocompatibility.

Alloying has been acknowledged as an effective approach to improve the mechanical properties and corrosion resistance of magnesium alloy implants. The main alloying elements include Yttrium(Y), Lithium(Li), Zirconium(Zr), Nickel(Ni), Copper(Cu), Zinc(Zn) and Manganese(Mn)[9,10,24–27]. However, some dissolved metal ions may adversely affect the cells of surrounding tissues. According to the previous research, alloying elements can be mainly classified into three categories, i.e. slightly, moderately and severely harmful elements[28]. Y, Li and Zr elements show slightly or moderately adverse effects while Ni, Cu, Zn and Mn elements have severely adverse effects on human bodies[28,29]. Although only the slightly or moderately toxic elements are allowed to be used in the production of magnesium alloy-based orthopedic implants, their concentrations should be maintained at a low level far below their threshold values to minimize the untoward effects caused by high concentration[30], which limits their further application in the medical magnesium alloy implants. Therefore, an alternative way should be adopted to improve the corrosion resistance of biodegradable Mg-based implants.

In fact, the surface of magnesium-based implants interacted with the physiological environment like body fluids is usually the area where the corrosion attack initiates[31]. Therefore, surface modification would be a

[1]Power Metallurgy Research Institute, Central South University, Changsha City 410083, Hunan Province, P.R. China. [2]Department of Pharmacy, School of Medicine, Ruijin Hospital, Shanghai Jiao Tong University, Shanghai 200003, P.R. China. [3]National Engineering Research Center of Light Alloy Net Forming, Shanghai Jiao Tong University, Shanghai 200240, P.R. China. [4]Inner Mongolia Research Institute, Shanghai Jiao Tong University, Hohhot 010010, P.R. China. [5]Shanghai Jiao Tong University Baotou Institute of Material Research, Baotou 014000, PR China. [6]Shanghai Key Laboratory of Hydrogen Science & Center of Hydrogen Science, Shanghai Jiao Tong University, Shanghai 200240, China. ✉email: fm04197@rjh.com.cn; fateratory@sjtu.edu.cn; weigl010@sjtu.edu.cn

feasible strategy to decrease the degradation rate of implants. Many researchers have found that the organic compounds coating such as proteins, carbohydrates and amino acids[32–38], which usually have the advantages of high biocompatibility, biodegradability and innocuity, can be regarded as potential candidates in promoting corrosion resistance of Mg-based implants. Liu et al.[39] studied the corrosion behavior of AZ91 alloy in simulated body fluids (SBF) with albumin addition and found that an enhanced corrosion resistance could be obtained in the albumin-containing SBF as compared with the albumin-free SBF. Chu et al.[40] reported that there is a reduction in the corrosion and hydrogen evolution rate of Mg-Ca alloy when immersing alloy into the bovine serum albumin containing saline. The similar phenomenon was observed by Hornberger et al.[41], who concluded that the fetal calf serum addition has a positive effect on the corrosion behavior of WE43 alloy. The corrosion inhibition can be attributed to the barrier effect of albumin molecules absorbed on the metal surface, which form a protective protein layer between the metal and the surrounding environment[31,40,42]. In addition, glucoses were found to be effective in improving the corrosion resistance of magnesium alloy by forming calcium phosphate compound on its surface in hank's solution[36,43,44]. Fructose also exhibits an ability of strengthening phosphates deposition on AZ31 alloy surface to increase its degradation resistance[45]. Moreover, the amino acids like L-cysteine were investigated and confirmed to increase the anti-corrosion performance of AZ31 alloy[35]. The corrosion inhibition may be due to the L-cysteine-bioinspired calcium phosphate (Ca-P) coating on the surface of magnesium.

Despite the corrosion inhibition effect, some problems or challenges are still posed in the application of these organic compounds. Firstly, it is documented that proteins show an alloy-dependent and time-dependent complicated behavior. Gu et al.[46] suggested that the serum protein can accelerate the corrosion of Mg-Ca alloy, and it can also accelerate the corrosion of AZ31 in the initial 3 days but decelerate it thereafter with the serum addition, while AZ91 alloy exhibits a reduced corrosion rate upon addition of serum to Hank's solution. Secondly, it is reported that glucose demonstrates a concentration-dependent effect on the degradation behavior of magnesium in Hank's solution[44,47], i.e. as the content of glucose increases, the corrosion resistance of magnesium decreases. Furthermore, amino acids may aggravate the dissolution of magnesium in the SBF solution by the chelating effect with Mg cations[45,48–50]. Therefore, more research is needed to further our understanding of the organic compounds-induced corrosion inhibition behavior of Mg-based orthopedic implants.

Studies show that patients with some diseases like hypertension are more likely to develop osteoporosis than the general population and some of them may experience the orthopedic surgery therapy[51–53]. Thus, a specialized treated Mg-based orthopedic implants would be the first choice for these patients. Nowadays, there are numerous antihypertensive drugs supplied for patients with hypertension[54–56]. These drugs are basically composed of organic compounds. If some of them are capable of adsorbing on the surface of magnesium alloys to suppress corrosion, as the albumin molecules absorb on the surface of AZ91 alloy, it may provide a potential avenue for enhancing the anti-corrosion performance of Mg-based orthopedic implants for hypertensive patients. However, few research has been focused on the effects of antihypertensive drugs on the corrosion behavior of Mg-based orthopedic implants and the underlying corrosion inhibition mechanisms have not yet been clarified.

In the present study, seven common antihypertensive drugs named *Losartan Kalicum*(LK), *Atenolol*(ATEN), *Nifedipine*(NF), *Hydrochlorothiazide*(HCTZ), *Valsartan*(VLA), *Furosemide*(FUR) and *Captopril*(CAP) were selected to investigate their effects on the corrosion behavior of AZ31 alloy. In vitro corrosion experiments in simulated body fluid (Hank's solution)[57] were performed. The outcome of this work may provide new idea and approach to the development of Mg based orthopedic implants with high corrosion resistance.

Experiments

Materials preparation

As one of the most widely studied magnesium alloys in biomedical field, AZ31 alloy with well-established degradation behavior and mechanical properties was used in this work. Although AZ31 contains ~ 3 wt% Al, studies[17,26] have shown that aluminum ion release during degradation is minimal and remains below cytotoxic levels, especially in short-term and localized orthopedic use. Moreover, Al mainly exists in stable intermetallic phases, which further limits its release. Commercial extruded AZ31 alloys were purchased from Dongguan Brilliant Special Metal Processing Co.,Ltd., China. Samples for electrochemical experiments were machined into cylinders with size of 14 mm in diameter and 5 mm in height. The samples used for corrosion immersion tests were machined into the cuboids with size of 1 cm ×1 cm× 0.5 cm. All samples prior to all experiments were all grounded with emery-paper of #300, #1200, #3000 and #5000 grits, rinsed in ethanol with ultrasonication assistance and then dried in hot air. The molecular structure and chemical formula of seven antihypertensive drugs *Losartan Kalicum*(LK), *Atenolol*(ATEN), *Nifedipine(*NF), *Hydrochlorothiazide* (HCTZ), *Valsartan*(VLA), *Furosemide*(FUR) and *Captopril*(CAP) are displayed in Fig. 1. All drugs were supplied from Department of Pharmacy, Ruijin Hospital in forms of powder.

Solution preparation

The Hank's solution was selected as in-vitro corrosion experiments environment and the main component of solution is listed in Table 1. Seven antihypertensive drug powders with the concentration of 1.0 g/L were respectively added into Hank's solution for the preliminary anticorrosion performance screening. A blank solution without any antihypertensive addition was also investigated for comparison. Besides, the screened antihypertensives with different addition levels were also added into Hank's solution to explore the influence of addition level on the corrosion behavior. It is noted that the antihypertensives were applied as corrosion inhibitors for Mg-based orthopedic implants and the drug concentration selection is based on the corrosion properties of AZ31 magnesium alloy in Hank's solution instead of therapeutic plasma levels. The drug concentration widely adopted in clinical practice is more suitable for further in vivo experiments.

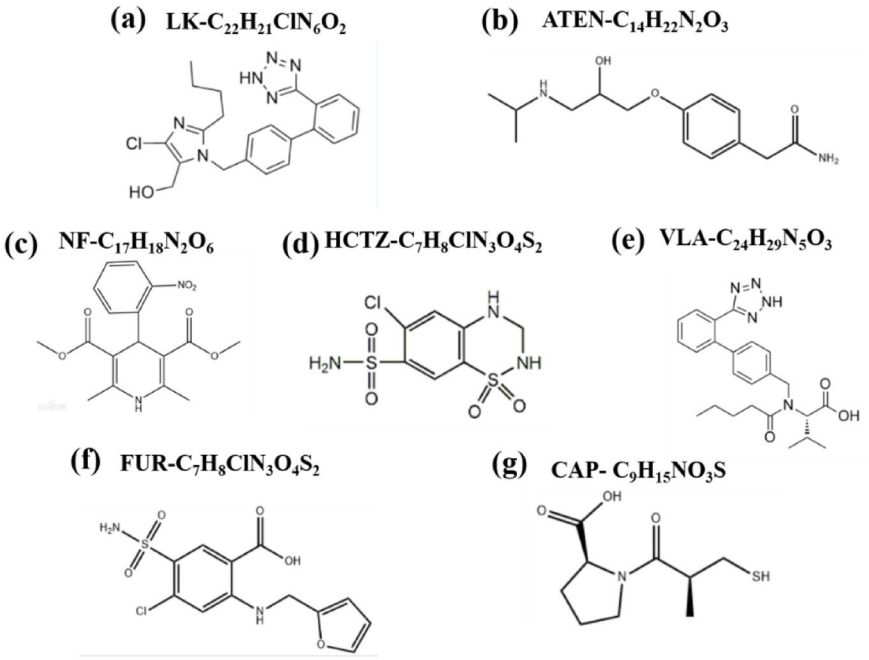

Fig. 1. Molecular structure of seven antihypertensive drugs. (**a**) LK; (**b**) ATEN; (**c**) NF; (**d**) HCTZ; (**e**) VLA; (**f**) FUR; (**g**) CAP;.

System	R_s (Ω cm^2)	Rct (Ω cm^2)	R1 (Ω cm^2)	R2 (Ω cm^2)	R_p (Ω cm^2)	C (10^{-7} F)	CPE1(10^{-5} S s^n cm^{-2})	n1	CPE1(10^{-5} S s^n cm^{-2})	n2	η_{EIS} (%)	-Ecorr (mV)	Icorr (μA cm-2)	η_{Icorr} (%)
Blank	41.61	35.02	6789	1397	8262.63	4.968	1.436	0.7962	52.9	1	-	1330	1.849	-
LK	43.04	28.18	7866	4757	12694.22	2.682	1.396	0.8009	13.64	1	**34.9**	1246	1.387	**24.9**
ATEN	10.93	52.68	3620	1265	4948.61	5.978	1.064	0.9224	7.1	0.7412	**−66.9**	1357	2.467	**−33.4**
NF	60.82	47.59	21,820	4521	26449.41	5.617	1.191	0.8047	28	1	**68.8**	1288	0.565	**69.4**
HCTZ	70.98	38.43	918	13,580	14607.41	2.747	1.451	0.7096	21.64	1	**43.4**	1282	0.942	**49.1**
VLA	37.91	43.86	2502	491.8	3075.57	0.105	2.466	0.8078	321.8	0.9938	**−168.6**	1384	2.217	**−19.9**
FUR	68.87	46.98	6045	696.3	6857.15	7.551	1.35	0.8189	221.9	0.9931	**−20.4**	1348	1.919	**−3.7**
CAP	10	47.8	1398	372.8	1828.6	0.215	1.641	0.8957	198.2	0.8398	**−351.8**	1363	7.087	**−283.2**

Table 1. Corresponding fitted parameters of PDP curves and EIS spectra of AZ31 alloy in hank's solution with addition of 1.0 g/L of seven antihypertensives, respectively.

Corrosion tests

Hydrogen evolution

Hydrogen evolution experiments were carried out on the 1 cm^2 area of AZ31 alloy cuboids using eudiometers. The tested samples were all inlaid in epoxy resin with a surface exposed. The volume of hydrogen evolution was recorded at the duration time of 7 days. The corrosion rate $V_{He\ (mm/yr)}$ determined by hydrogen evolution is given by following Eqs[58,59]. :

$$V_{He} = 2.088\frac{V_H}{At} \tag{1}$$

where V_H (mL) is the volume of evolved hydrogen, A (cm^2) is the surface area of samples and t (day) is the immersion duration.

Weight loss

The weight loss tests were adopted on AZ31 alloy immersed in Hank's solution with and without antihypertensives. All samples were pre-weighed and reweighed after different immersion time. The weight loss was recorded at the duration time of 1, 3, 5 and 7 days, respectively. The corrosion rate V_{wl} (mm/yr) indicated by weight loss is calculated by given equation[60]:

$$v_{wl} = 8.74 \times 10^4 \times \frac{m_1 - m_2}{A_s \cdot t \cdot d} \tag{2}$$

where m_1 and m_2 is the sample mass before and after immersion, respectively. A_s (cm^2) is the contact surface area between solution and samples, t(h) is the duration time and d(g/cm^3) is the density of alloy. Note that the exposed surface area of 4 cm^2 of samples were applied for weight loss tests.

Electrochemical experiments
A DH7000 Electrochemical Workstation was used for the electrochemical measurements including open circuit potential (OCP), electrochemical impedence spectroscopy (EIS) and potentiodynamic polarization (PDP). The experimental instrument is composed of a three-electrode cell, AZ31 sample as the working electrode, a platinum sheet as a counter electrode and a saturated KCl electrode as a reference electrode. The test area of all samples is a circle with diameter in 14 mm. The EIS measurements were conducted in the frequency range of 100,000 Hz to 0.01 Hz. The PDP experiments were performed at the potential of ± 0.3 V vs. OCP with a scan rate of 1 mVs^{-1}. Before the EIS and PDP experiments, the OCP was measured for duration time of 30 min to obtain a pseudo steady state condition. The analysis of EIS and PDP data were done using Z-view and EC-lab software, respectively.

Materials characterization

The morphologies of the corroded surface of AZ31 alloy after immersion in Hank's solution with and without antihypertensives and the elemental composition of the products on the surfaces were determined using a TESCAN- MAIA3 scanning electron microscopy (SEM) coupled with energy-dispersive X-ray spectroscopy (EDS). The voltages of 5 kV and 15 kV were adopted for morphology observation and EDS mapping, respectively. A Poly-functional X-Ray Diffractometer (XRD) with voltage of 40 kV and current of 40 mA was used for phase identification. The step size is 0.02° and the scan angles is a range of 10–90°. The roughness of corroded sample surface was characterized by Ultra-Depth Three-Dimensional Microscope (KEYENCE, VHK-7000). X-ray photoelectron spectroscopy (XPS) studies were performed utilizing AXIS UltraDLD XPS spectrometer to analyze the information of elements and their valence states of corroded surface of AZ31 alloy. A fourier transform infrared (FTIR) spectrophotometer and Raman spectroscopy were used to investigate the chemical structure and surface functional groups on the corroded AZ31 alloys.

Results and discussion

Corrosion behavior of AZ31 alloy influenced by seven antihypertensives

The electrochemical experiments were firstly carried out on the AZ31 alloy in Hank's solution without and with seven antihypertensive drugs with a concentration of 1 g/L to screen out which one shows a positive effect on the corrosion inhibition and the related results are displayed in Fig. 2. It can be seen from PDP curves in Fig. 2(a) that three curves corresponding to the solutions with the addition of LK, NF and HCTZ exhibit a more positive position than blank solution, and the other four curves of solutions with ATEN, VLA, FUR and CAP addition shift toward negative position than blank solution. A more positive curve means a higher corrosion potential, indicating a better corrosion resistance. Furthermore, the corrosion current density is also an important indicator to evaluate the corrosion behavior. The quantitative corrosion potential (E_{corr}) and corrosion current density (I_{corr}) can be analyzed by Tafel fitting and the results are listed in Table 1. It is apparent that the I_{corr} values of the solutions with the addition of LK, NF and HCTZ are all smaller than blank solution, which reveals that the corrosion reaction can be effectively suppressed by these three antihypertensives. Among them, the smallest corrosion current density can be obtained in NF-contained solution.

Figure 2 (b) exhibits EIS spectra for different antihypertensives. It is observable that the larger semi-circle of Nyquist plots are achieved upon addition of LK, NF and HCTZ, manifesting their better anti-corrosion performance. The bode diagrams and bode phase diagrams are also exhibited in Fig. 2(c) and (d), respectively. It can be seen that the higher impendence can be obtained in the solutions containing LK, NF and HCTZ antihypertensives, whether in low frequency or high frequency regions. The higher value of modulus |Z| at low frequency represents lower degradation rate[61]. In order to further understand the effect of antihypertensives on the degradation behavior of AZ31 alloy, a selected equivalent circuit model demonstrated in Fig. 2(e) was used for EIS curves fitting and the relevant fitting data are listed in Table 1. The consistency between fitted results and original curves in Fig. 2(f) guarantees the veracity of the used equivalent circuit model. In this equivalent circuit model, R_s is the resistance of solutions, R_{ct} stands for the charge transfer resistance, R_{f1} and R_{f2} are the film resistance on the surface of AZ31. The constant phase angle element (CPE) is usually used to simulate electric double layer due to dispersed activation energy distribution effect and the roughness and inhomogeneity of the electrode surface. C is the capacitance of the system. The corrosion performance can be quantitatively assessed by polarization resistance (R_P), which is given by Eq. (3)[62]:

$$\frac{1}{R_P} = \frac{1}{R_{ct} + R_{f1} + R_{f2}} \tag{3}$$

The improved corrosion resistance efficiency influenced by antihypertensives can be calculated by Eqs. (4) and (5)[62,63]:

$$\eta_{EIS} = \left(\frac{R_{PA} - R_{PB}}{R_{PA}}\right) \times 100\% \tag{4}$$

$$\eta_{Icorr} = \left(\frac{I_{corr(B)} - I_{corr(A)}}{I_{corr(B)}}\right) \times 100\% \tag{5}$$

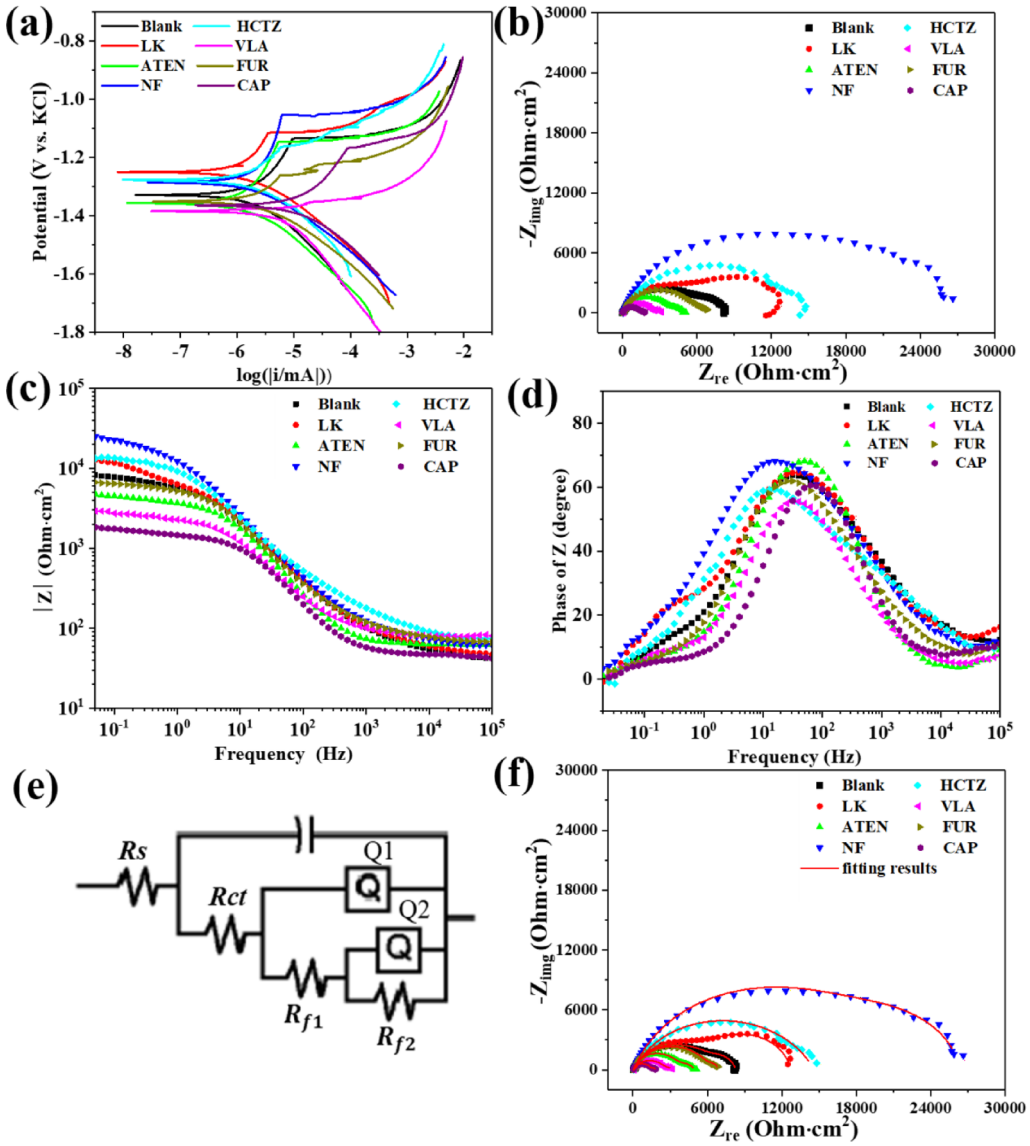

Fig. 2. Electrochemical tests of AZ31 alloy in Hank's solution without and with seven antihypertensive drugs with concentration of 1 g/L. (**a**) Potentiodynamic polarization curves; (**b**) Electrochemical impedance spectra; (**c**) Bode diagrams; (**d**) Bode phase diagrams; (**e**) Applied equivalent circuit model; (**f**) Comparisons between original data and fitted results of EIS curves.

where η_{EIS} corresponds to the improved efficiency based on EIS experiments, R_{PA} is the polarization resistance of AZ31 alloy immersed in Hank's solution with addition of antihypertensives and R_{PB} is the polarization resistance of AZ31 alloy immersed in blank Hank's solution. η_{Icorr} refers to the improved efficiency based on PDP tests, $I_{corr(B)}$ is the corrosion current density of the AZ31 alloy immersed in blank Hank's solution and $I_{corr(A)}$ is the corrosion current density of AZ31 alloy immersed in Hank's solution with addition of antihypertensives. As shown in Table 1, the polarization resistance of LK, NF and HCTZ are higher than that of blank solution. By calculation, the η_{EIS} value of LK, NF and HCTZ are 34.9%, 68.8% and 43.4%, respectively. Similarly, the corrosion density of LK, NF and HCTZ are smaller than that of blank solution and the improved efficiency η_{Icorr} are 24.9%, 69.4% and 49.1%, which are basically consistent with the EIS results. These quantitative results provide strong evidences that LK, NF and HCTZ can effectively inhibit corrosion and reduce the degradation rate of AZ31 alloy, among which NF has the highest efficiency. Interestingly, it can be seen from the Table 1 that there is no obvious variation in the value of solution resistance R_s and the charge transfer resistance R_{ct} of all antihypertensives as compared to blank solution. Conversely, a significant shift occurs in the value of film resistance. It can be reasonably speculated that the antihypertensives influencing the corrosion behavior of AZ31 alloy may be realized by altering protective capability of film formed on the alloy surface. LK, NF and HCTZ have a positive effect on film protection while other antihypertensives may weaken film protection by reducing its film resistance.

Immersion test results

Figure 3 exhibits the immersion test results of AZ31 alloy immersed in Hank's solution without and with LK, NF and HCTZ antihypertensives with a concentration of 1 g/L for seven days. As shown in Fig. 3(a), The weight-loss of AZ31 alloys in four solutions were recorded at the interval of 1, 3, 5 and 7 days, respectively. The variation of weight loss for all alloys shows an increasing trend with the increase of time. The AZ31 alloy immersed in 1 g/L LK, NF and HCTZ antihypertensives containing solution reveals a slighter weight reduction as compared to that in blank Hank's solution, among which NF demonstrates the smallest weight-loss. Based on the Eq. (1), the corrosion rate of AZ31 alloy in blank solution is estimated to be 2.25 mm/yr. After adding 1 g/L LK, NF or HCTZ antihypertensives into solution, the corrosion rate is reduced to be 1.81, 1.12 and 1.28 mm/yr, respectively. The highest reduction of 50.2% can be achieved by addition of NF. Apart from weight-loss test, the volume evolution of hydrogen gas during immersion process has also been acknowledged as a persuasive method to assess the corrosion performance of magnesium alloy since the main corrosion products of the reduction reaction induced by magnesium in aqueous solution are H_2. Figure 3(b) shows the volume of hydrogen gas evolved from AZ31 alloy immersed in four solutions at a durable time of 7 days. It can be seen that two stages can be observed during the overall process. At initial two days of immersion, the hydrogen gas evolves at an unstable stage and the evolution rate is relatively high. Subsequently, an approximately linear relationship between the volume of evolved gas and the time can be observed, implying that the hydrogen evolution gradually tends to be steady as the immersion time increases. Furthermore, the evolution rate in second stage is also lower that in first stage. Compared with blank solution, the addition of LK, NF and HCTZ antihypertensives can effectively stifle the release of hydrogen no matter in first stage or second state. By adopting Eq. (2), the corrosion rate indicated by hydrogen evolution of AZ31 alloy in blank solution is 3.23 mm/yr and its value is decreased to be 2.76, 2.31 and 2.42 mm/yr upon addition of LK, NF and HCTZ antihypertensives, respectively. According to the immersion results above, it is clear that LK, NF and HCTZ are valid in inhibiting the corrosion of AZ31 alloy in Hank's solution. These results show a good agreement with the electrochemical measurements.

Morphologies of surface and cross-section of the AZ31 alloy after corrosion

Figure 4 displays the SEM surface morphologies of AZ31 alloy immersed in Hank's solution without and with LK, NF and HCTZ antihypertensives with a concentration of 1 g/L at a duration time of seven days. At the initial 1 day of immersion in blank Hank's solution in Fig. 4(a), some shallow and small cracks appear on the surface of AZ31 alloy. As the immersion time increases, the cracks in Fig. 4 (b) and (c) become deeper and larger, indicating that the corrosion of alloy is gradually worsened. The widest and largest cracks can be seen in the alloys upon the condition of seven days of immersion, as exhibited in Fig. 4(d). After incorporating LK, NF and HCTZ antihypertensives into solutions, as indicated in Fig. 4 (e-h), Fig. 4(i-l) and Fig. 4(m-p), respectively, the corrosion of AZ31 alloy surfaces are effectively improved, whose surfaces are characterized by smaller and tinier cracks as compared to that immersed in blank Hank's solution at any immersion time. Especially for NF, the cracks are not obvious and discernible until after five days of immersion. In addition, it can be also seen that there are more corrosion products distributed on the surface of corroded AZ31 alloy in all solutions. A more uniform surface film formed on the surface of alloy in NF-contained solution demonstrated in Fig. 4(l) indicates a better protection effect on the corrosion propagation, which is in agreement with high film resistance analyzed by EIS technique. Figure 5 are the EDS mapping results of surface of AZ31 alloy immersed in Hank's solution without and with LK, NF and HCTZ antihypertensives with a concentration of 1 g/L for seven days. It indicates that the surface films of AZ31 alloy immersed in four solutions are all composed of Mg, O, P, Ca, C, Al and Na. Compared with blank Hank's solution, the contents of Ca and P in the surface film show a significant increase after addition of antihypertensives. The Ca content changes from 4.57 wt% in blank Hank's solution to 11.33, 22.24, and 18.09 wt% in LK, NF and HCTZ containing solutions, respectively, and the P content increases from

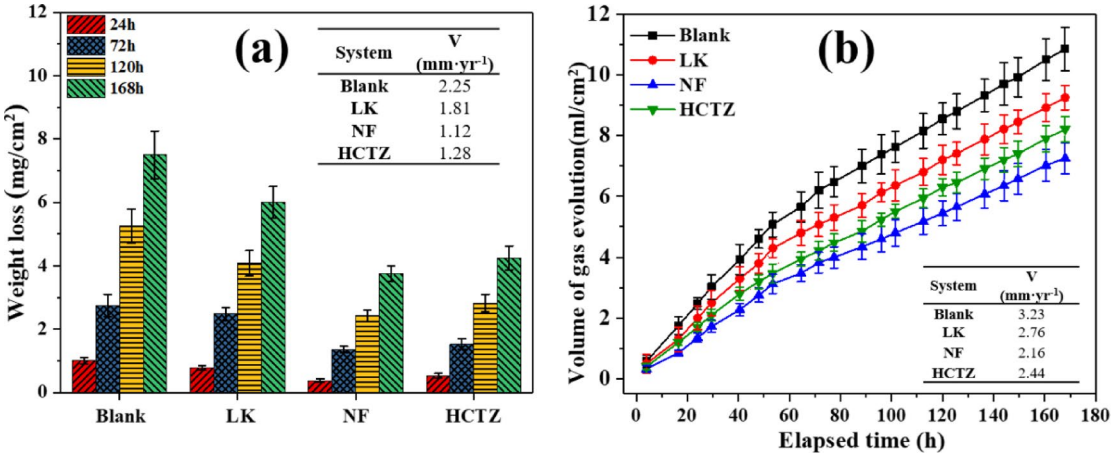

Fig. 3. Immersion tests of AZ31 alloy immersed in Hank's solution without and with LK, NF and HCTZ antihypertensives with concentration of 1 g/L for seven days. (**a**) Hydrogen evolution volume as function of elapsed time; (**b**) Wight-loss at different time intervals.

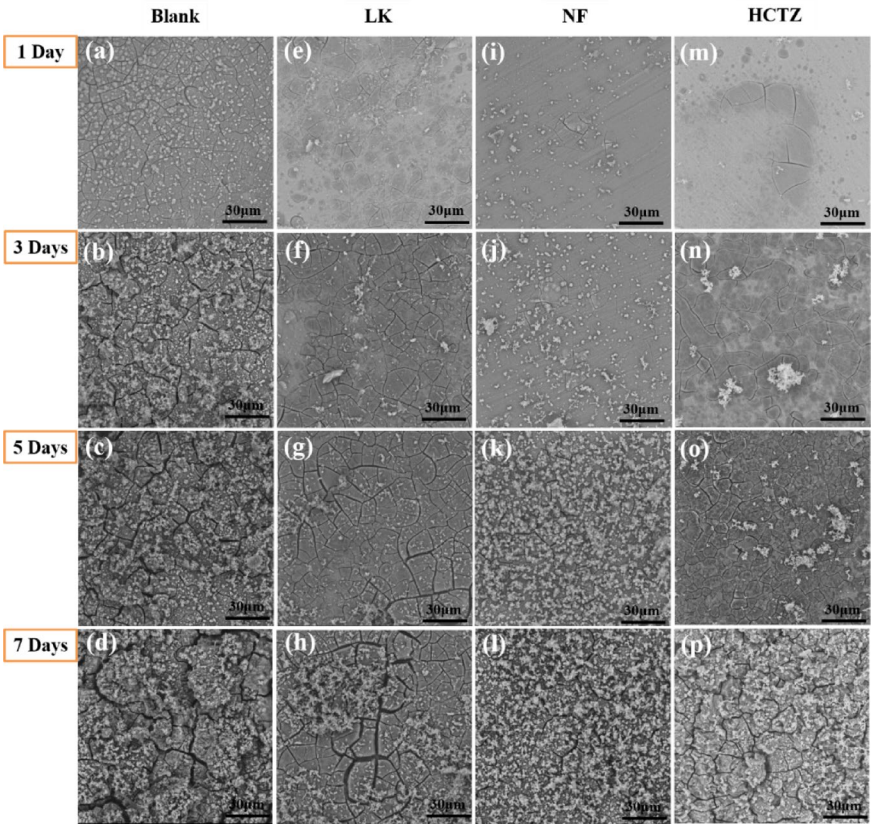

Fig. 4. SEM surface morphologies of AZ31 alloy immersed in Hank's solution without and with LK, NF and HCTZ antihypertensives with concentration of 1 g/L at a duration time of seven days (**a**-**d**) Blank solution; Hank's solution with addition of (**e**-**h**) LK, (**i**-**l**) NF and (**m**-**p**) HCTZ.

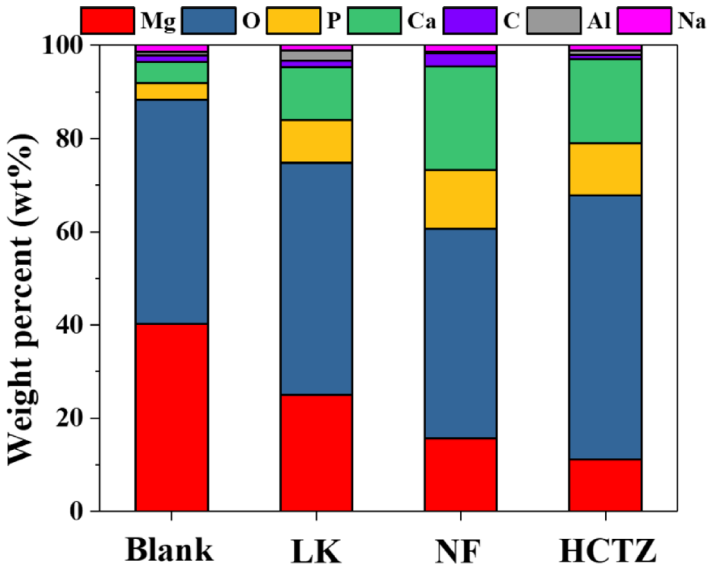

Fig. 5. EDS mapping results of surface of AZ31 alloy immersed in Hank's solution without and with LK, NF and HCTZ antihypertensives with concentration of 1 g/L for seven days.

3.54 wt% to 9.12, 12.67 and 11.22 wt%, respectively. Actually, Ca and P are present in the form of Ca-P apatite, which is beneficial to protective capability of surface film. The higher Ca and P contents signify the increment of Ca-P apatite, thus leading to the higher resistance of film to corrosion. As a result, the degradation rate of AZ31 alloy would be greatly reduced. Overall, it can be reasonably concluded that the addition of LK, NF and

HCTZ antihypertensives are capable of promoting the formation of Ca-P apatite on the surface of AZ31 alloy. It is worth noting that, based on the EDS results shown in Fig. 5 and the calculation of the Ca/P ratio, Ca-P apatite is identified as hydroxylapatite.

Figure 6 displays the cross-sectional SEM images of AZ31 alloy immersed in Hank's solution without and with LK, NF and HCTZ antihypertensives with a concentration of 1 g/L at a duration time of seven days. As shown in Fig. 6 (a-d), the thickness of corrosion layer of AZ31 samples immersed in blank Hank's solution gradually increases with the extension of immersion time from 1 to 7 days. The numerous horizontal and vertical cracks can be evidently observed in these layers. With the addition of LK into solution, as exhibited in Fig. 6(e-h), the thickness of corrosion layers is greatly reduced at all immersion time and these layers seem to be more homogeneous compared with that in blank Hank's solution. Furthermore, there is a remarkable decrease in the number density of cracks within the corrosion layers. The same effect can be also discovered in the NF and HCTZ containing solutions and the relevant results are disclosed in Fig. 6(i-l) and Fig. 6(m-p), respectively. The maximum thicknesses of corrosion layer of AZ31 alloy immersed in four solutions for seven days are 203.3, 94.5, 62.7 and 84.8 μm, respectively. The thinnest corrosion layer is obtained in NF-contained solution, confirming its optimal corrosion resistance. The experimental results above provide a convincing evidence that the LK, NF and HCTZ antihypertensives can act as an effective surface modifier to improve the corrosion resistance of AZ31 alloy implants.

Figure 7 shows the optical images, 2D and 3D topographies and surface roughness (S_a) characteristics of the corroded surface of AZ31 alloy after immersing in Hank's solution without and with LK, NF and HCTZ antihypertensives with a concentration of 1 g/L for seven days. The surface roughness can be deemed as a pivotal indicator to evaluate the extent to which the corrosion occurs on the alloy surface. As shown in Fig. 7(a), it can be seen that a severe corrosion attack happens on the surface of AZ31 alloy immersed in blank Hank's solution. The analyzed 3D topography is characterized by a rugged corroded surface with numerous visible deep valleys and high peaks. By measurement, its surface roughness is estimated to be 0.946 μm. When immersing the AZ31 alloy

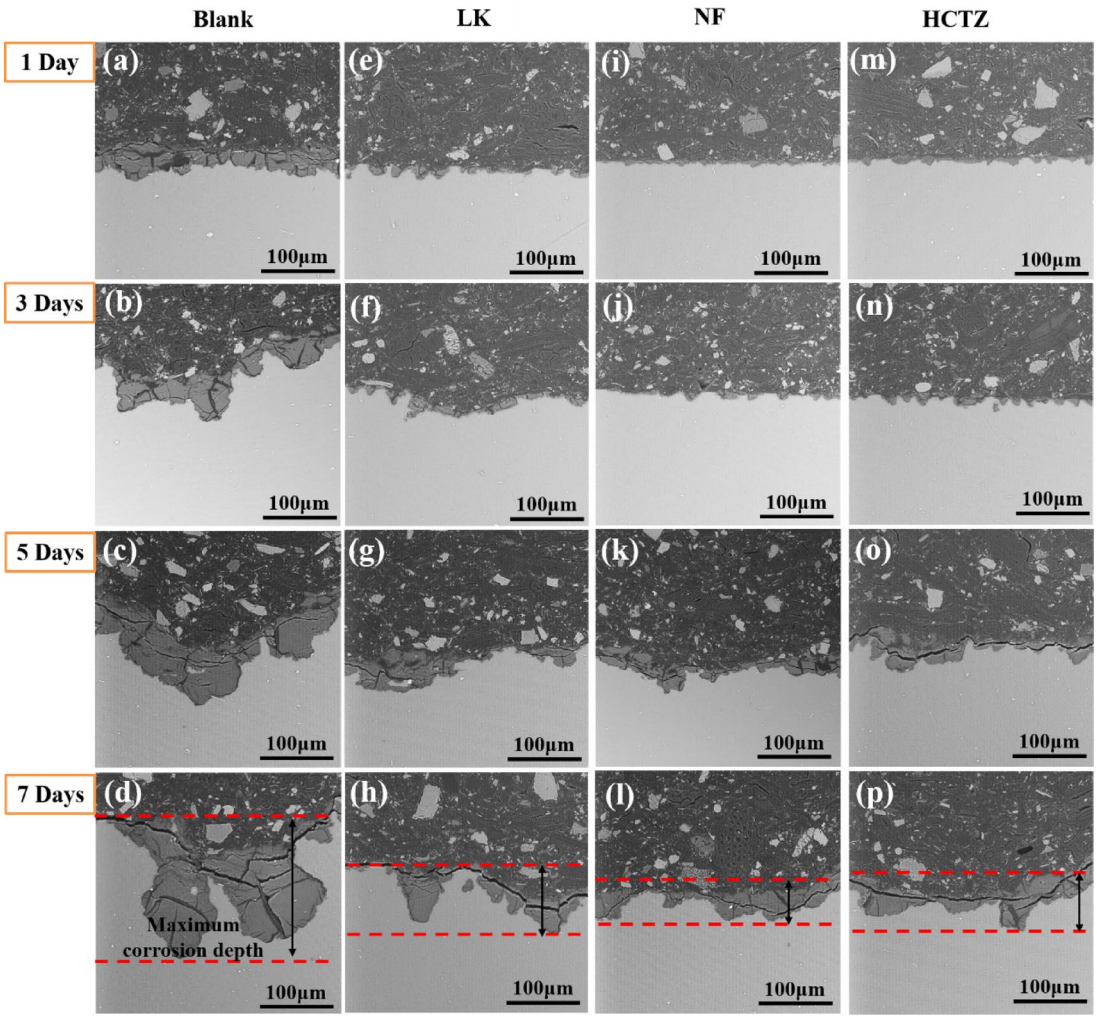

Fig. 6. Cross-sectional SEM images of AZ31 alloy immersed in Hank's solution without and with LK, NF and HCTZ antihypertensives with concentration of 1 g/L at a duration time of seven days. (**a**-**d**) Blank solution; Hank's solution with addition of (**e**-**h**) LK, (**i**-**l**) NF and (**m**-**p**) HCTZ.

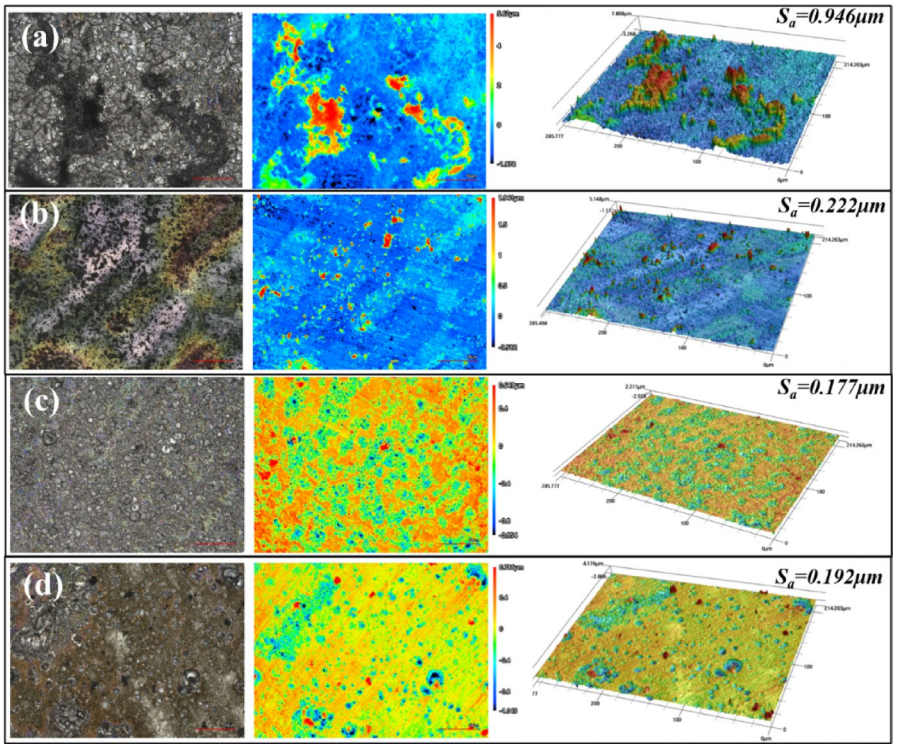

Fig. 7. Optical images, 2D and 3D topographies and surface roughness (Sa) characteristics of the corroded surface of AZ31 alloy after immersing in Hank's solution without and with LK, NF and HCTZ antihypertensives with concentration of 1 g/L for seven days(**a**-**d**) Blank solution; Hank's solution with addition of (**e**-**h**) LK, (**i**-**l**) NF and (m-p) HCTZ.

into the antihypertensives containing solution, the corroded surface of AZ31 alloy become more smooth and flat and there is an obvious reduction in the size and number of valleys and peaks located on surface. Compared with LK and HCTZ, a flattest topography can be observed in the solution with NF addition, which implies a slightest corrosion on alloy surface. The surface roughness of AZ31 alloy immersed in LK, NF and HCTC-contained solution are calculated to be 0.222, 0.177, and 0.192 μm, respectively, showing a decrease of 76.5, 81.2, and 79.7% as compared to that in blank Hank's solution. It can be reasonably concluded that the antihypertensives of LK, NF and HCTZ evince a remarkable anti-corrosion performance on AZ31 alloy in simulated body fluid environment. By comparison with LK and HCTZ, NF possesses the greatest ability of retarding the degradation rate of AZ31 alloy, which is concordant with electrochemical and immersion test results.

Analysis of corrosion film products on surface of AZ31 alloy

Figure 8 exhibits the XRD patterns of corroded surface of AZ31 alloy after immersing in Hank's solution without and with LK, NF and HCTZ antihypertensives with a concentration of 1 g/L for seven days. It can be seen that four phases can be detected from the spectral results in four different solutions, referring to Mg, MgCO3, $Mg(OH)_2$ and hydroxylapatite, respectively. The existence of $MgCO_3$ may be due to the reaction between $Mg(OH)_2$ and CO_2 in atmosphere environment. The weak intensity of diffraction peaks of $Mg(OH)_2$ can be revealed in blank solution, meaning that the crystallinity of $Mg(OH)_2$ is not sufficient. After adding antihypertensives, there is an increase in the peak intensity and a decrease in the peak width of $Mg(OH)_2$, which demonstrates that these three antihypertensives may promote the crystallization of magnesium hydroxide to some extent. The higher crystallinity of $Mg(OH)_2$ may improve the integrity of corrosion film on the alloy surface to impede corrosion attack. Furthermore, apart from obvious Mg peaks, several strong peaks of hydroxylapatite at the 2-Theta ranging from 20° to 50° can be evidently seen in all solutions. Compared with blank solution, the peak intensity of hydroxylapatite appears stronger in the solution with addition of antihypertensives. Especially for NF-contained solution, it shows a relatively strongest peak intensity of hydroxylapatite among three antihypertensives, which is consistent with EDS mapping results. Therefore, it can be safely speculated that the antihypertensives are effective in facilitating the formation of hydroxylapatite precipitates on the corrosion surface.

To further investigate the surface element state of corroded surface, XPS analysis was conducted on AZ31 alloy after the immersion time of seven days in Hank's solution without and with LK, NF and HCTZ antihypertensives with a concentration of 1 g/L and the corresponding fitting results are displayed in Fig. 9. Figure 9(a-e) shows the high-resolution spectrum of Mg 1 s, O 1 s, C 1 s, Ca 2p and P 2p of corrosion products located on the surface of AZ31 alloy immersed in blank Hank's solution. The binding energy peak of C 1 s at 1303.54 eV and 1304.59 eV corresponds to $Mg(OH)_2$ and $MgCO_3$[64], respectively. From the O 1 s spectra, the P = $O/CO3^{2-}$ peak at 532.79 eV[65] and OH^- peak at 531.46 eV can be obviously observed. The fitting results of C 1 s clearly demonstrates

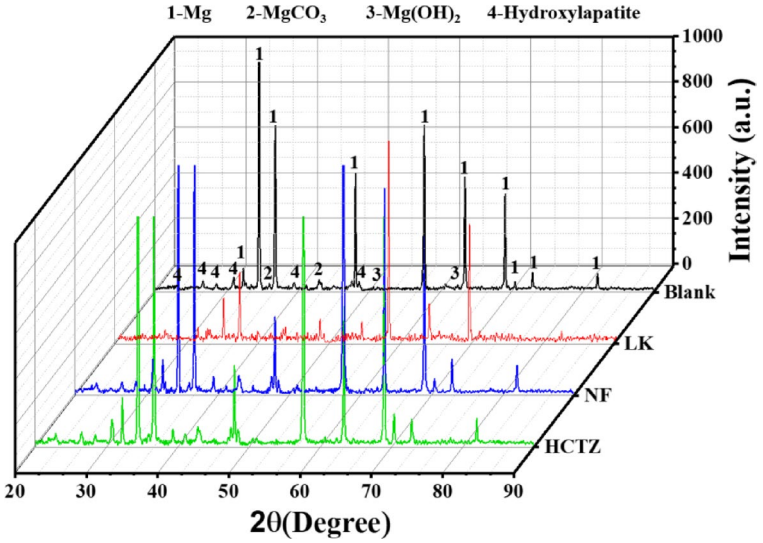

Fig. 8. XRD patterns of corroded surface of AZ31 alloy after immersing in Hank's solution without and with LK, NF and HCTZ antihypertensives with concentration of 1 g/L for seven days.

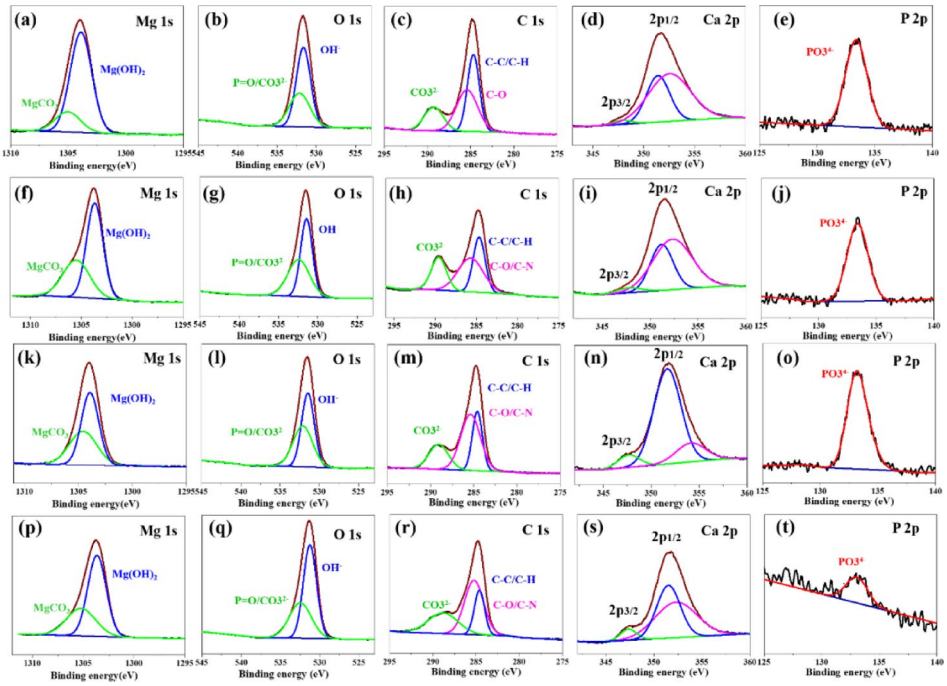

Fig. 9. XPS analysis of surface of AZ31 alloy after immersion time of seven days in Hank's solution without and with LK, NF and HCTZ antihypertensives with concentration of 1 g/L. (**a**-**e**) Blank solution; Hank's solution with addition of (**f**-**j**) LK, (**k**-**o**) NF and (**p**-**f**) HCTZ.

three functional group components for corrosion products. The peak emerged at 284.52 eV can be assigned to C-C/C-H bond, the peak raised at 285.35 eV can be identified to C-O bond[66] and the peak elevated 289.08 eV can be associated with $CO3^2$ bond. In high-resolution XPS of Ca 1 s, the binding energy peak Ca 2p3/2 and the satellite peak Ca 2p1/2 can be detected from the spectra. It can be seen that the binding energy peak Ca 2p3/2 is consistent with the fitting peak at 347.6 eV, which refers to the existence of hydroxyapatite[45]. In addition, the XPS spectra of P 2p also indicates a $PO3^{4-}$ peak at binding energy of 133.74 eV[67], confirming the formation of hydroxyapatite. After incorporating LK, NF and HCTZ antihypertensives into the solution, as exhibited in Fig. 9(f-j), Fig. 9(k-o) and Fig. 9(p-t), respectively, the high-resolution spectra of Mg 1 s, O 1 s, Ca 2p and P 2p present the same characteristics of binding energy peaks as those in the blank solution. It should be noted that there is a difference in the energy peak of C-O bond in C 1 s spectra. The fitting peaks colored with pink is associated with

C-O bond in blank solution. However, according to the molecular composition of antihypertensives in Fig. 1, the C-N bond would be introduced when these antihypertensives are added into solution. The relative intensity of pink fitting peaks located at 285.93 eV in Fig. 9(h), 285.83 eV in Fig. 9(m) and 285.91 eV in Fig. 9(r) all exhibit a higher value than C-O bond peak in blank solution, revealing that the pink fitting peaks in LK, NF and HCTZ-contained solution is the combination of C-O bond and C-N bond rather than single C-O bond. Wei et al.[68]. also reported that the C-N peak exhibits the same binding energy position with C-O peak. Hence, the existence of C-N bond confirms that the antihypertensives may be involved in the formation of corrosion film on the surface of AZ31 alloy. In addition, the binding energy peak of Ca 2p3/2 appears to be more weak in blank solution as compared to that in antihypertensives-contained solution, signifying that more Ca-P apatites are formed under the influence of antihypertensives.

To differentiate hydroxyapatite from other calcium phosphates that may exhibit overlapping spectral features, Raman analysis[69–71] was conducted. Figure 10(a) presents the Raman spectra of AZ31 alloy after immersion for seven days in Hank's solution, both without and with the addition of the antihypertensive agents LK, NF, and HCTZ (each at a concentration of 1 g/L). In hydroxyapatite, a single intense $\nu_1$peak is typically observed at ~ 962 cm^{-1}. However, in some cases (e.g. β-Tricalcium phosphate), two peaks and a shoulder may appear due to structural variations. In the present work, only one peak near this wavenumber was detected. Moreover, in hydroxyapatite, the Raman scattering bands corresponding to the $\nu_2$and $\nu_4$modes are separated by approximately 120 cm^{-1}, which were also observed in the spectra. These features indicate that the final product is hydroxyapatite rather than other calcium phosphates. Complementary information was obtained from infrared (IR) spectra[72]. As shown in Fig. 10(b), the IR spectra of the same samples exhibit distinct absorption bands at 870 cm^{-1}, 1457 cm^{-1} and 1552 cm^{-1}, which are characteristic of B-type carbonated hydroxyapatite. These bands correspond to carbonate ions substituting for phosphate groups in the hydroxyapatite lattice. The presence of these characteristic peaks confirms the partial formation of B-type carbonated hydroxyapatite.

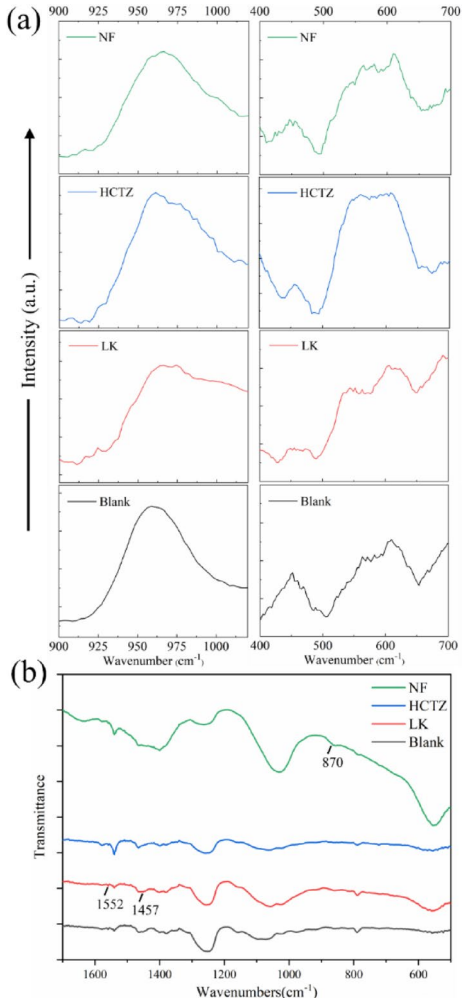

Fig. 10. (**a**) Raman spectra and (**b**) Infrared spectra of AZ31 alloy after immersion time of seven days in Hank's solution without and with LK, NF and HCTZ antihypertensives with concentration of 1 g/L.

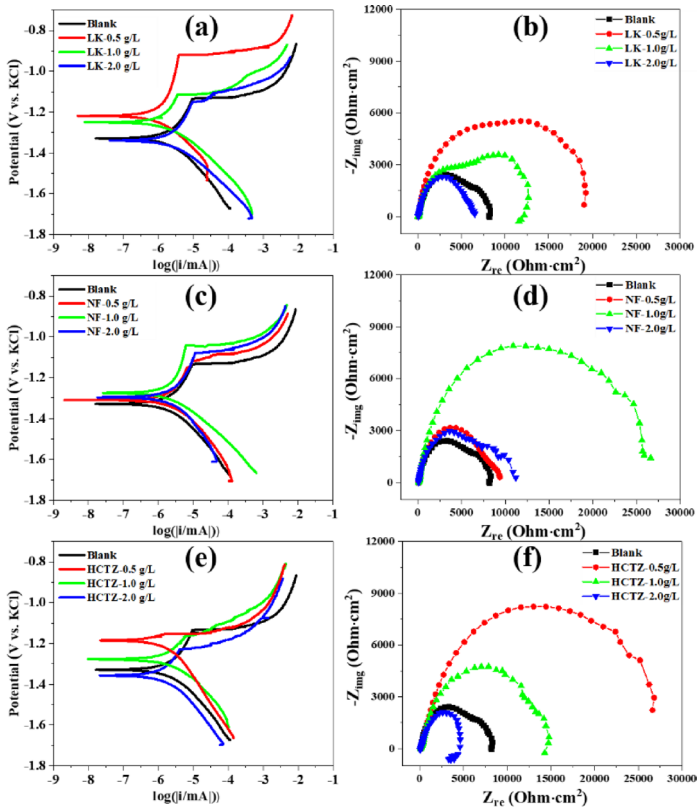

Fig. 11. Electrochemical characteristics of AZ31 alloy in Hank's solution with different concentrations of (**a**, **b**) LK, (**c**, **d**) NF, (**e**, **f**) HCTZ at normal temperature.

System	R_s (Ω cm²)	Rct (Ω cm²)	R1 (Ω cm²)	R2 (Ω cm²)	R_p (Ω cm²)	C (10^{-7}F)	CPE1(10^{-5} S s^n cm^{-2})	n1	CPE1(10^{-5} S s^n cm^{-2})	n2	η_{EIS} (%)	-Ecorr (mV)	Icorr (μA cm-2)	η_{Icorr} (%)
Blank	41.61	35.02	6789	1397	8262.63	4.968	1.436	0.7962	52.9	1	-	1330	1.849	-
LK-0.5 g/L	49.73	41.98	13,200	6213	19504.71	6.634	1.205	0.8395	13.72	0.9842	**57.6**	1218	0.683	**63.1**
LK-1.0 g/L	43.04	28.18	7866	4757	12694.22	2.682	1.396	0.8009	13.64	1	**34.9**	1246	1.387	**24.9**
LK-2.0 g/L	48.89	49.57	5824	519.4	6441.86	7.755	1.196	0.8431	265.9	1	**−28.2**	1339	1.967	**−6.2**
NF-0.5 g/L	50.18	58.34	8062	1118	9288.52	7.864	1.082	0.8457	133	1	**11.1**	1314	1.801	**2.5**
NF-1.0 g/L	60.82	47.59	21,820	4521	26449.41	5.617	1.191	0.8047	28	1	**68.8**	1288	0.565	**69.41**
NF-2.0 g/L	65.95	24.8	7593	2647	10330.75	7.361	1.326	0.836	31.5	1	**20.1**	1296	1.742	**5.7**
HCTZ-0.5 g/L	104.3	103	25,200	2752	28159.3	5.34	1.591	0.7436	52.6	1	**70.6**	1185	0.545	**70.5**
HCTZ-1.0 g/L	70.98	38.43	918	13,580	14607.41	2.747	1.451	0.7096	21.64	1	**43.4**	1282	0.942	**49.1**
HCTZ-2.0 g/L	102.1	146.1	1482	3244	4974.2	1.101	5.957	0.9067	0.644	0.9493	**−66.1**	1347	2.216	**−19.8**

Table 2. Corresponding fitted parameters of PDP curves and EIS spectra of AZ31 alloy in hank's solution with addition of different concentration of LK, NF and HCTZ, respectively.

The effect of antihypertensives concentration on AZ31alloy degradation behavior

To further clarify the concentration effect of LK, NF and HCTZ on the degradation behavior of AZ31 alloy, a wide range of addition levels from 0.5 to 2.0 g/L were taken into account. The electrochemical analysis was performed and the relevant results are plotted as Tafel and Nyquist curves in Fig. 11. The corresponding tafel fitting results and impedance fitting parameters are listed in Table 2. It can be seen from Fig. 11(a) that the polarization curves shift toward negative direction with increasing the concentration of LK from 0.5 to 2.0 g/L. According to the value of corrosion potential and corrosion current density in Table 2, the concentration of 0.5 g/L LK shows the greatest corrosion performance with the largest E_{corr} of −1218 mV and the smallest I_{corr} of 0.283 μA cm^{-2}. The higher concentration of LK may result in a decreased corrosion resistance, and the addition level of 2.0 g/L even cause a poorer corrosion than blank solution. It should be noted that the similar phenomenon can be observed in HCTZ containing solution where the concentration of 0.5 g/L exhibits the strongest corrosion inhibition effect and the addition of 2.0 g/L may accelerate corrosion process of AZ31 alloy, as displayed in Fig. 11(e). Unlike LK and HCTZ, the polarization curve of NF-containing solution in Fig. 11(c)

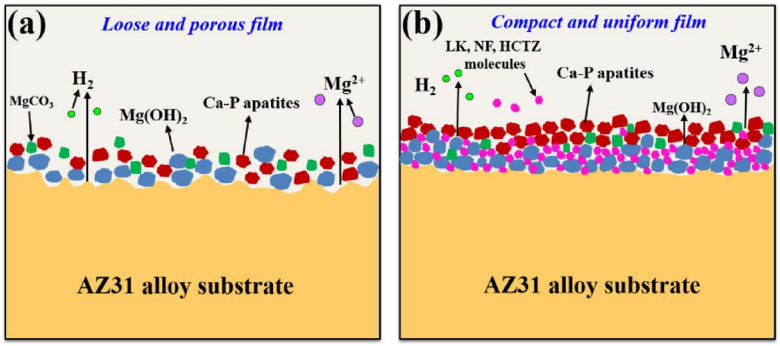

Fig. 12. Schematic diagrams of corrosion mechanisms of AZ31 alloy in Hank's solution without and with antihypertensives. (**a**) blank solution; (**b**) with addition of LK, NF and HCTZ.

firstly moves towards a positive direction as the concentration increases from 0.5 to 1.0 g/L and then goes down at an opposite direction when the concentration of NF continues to be increased to 2.0 g/L. The same variation is also revealed in the values of the corrosion potential and corrosion current density of NF-containing solution in Table 2. Based on the above results, the optimal addition levels of LK, NF and HCTZ for inhibiting corrosion of AZ31 alloy are 0.5, 1.0 and 0.5 g/L, respectively and their inhibiting efficiencies η_{Icorr} are calculated to be 63.1, 69.41 and 70.5%, respectively.

Figure 11(b), (d) and (f) show the variations of electrochemical impedance spectra with the concentration of LK, NF and HCTZ, respectively. The largest size of Nyquist semicircle can be obtained upon addition of 0.5 g/L of LK, 1.0 g/L of NF and 0.5 g/L of HCTZ, respectively, indicating the most pronounced corrosion protection. For LK, the polarization resistance of 0.5 g/L concentration is increased from 8262.63 Ω cm^2 in blank solution to 19504.71 Ω cm^2 and the inhibiting efficiency η_{EIS} is raised up to 57.6%. For NF, the highest polarization resistance of 26449.41 Ω cm^2 is demonstrated at the concentration of 1.0 g/L and the relevant η_{EIS} is determined to be 68.8%. For HCTZ, the strongest corrosion inhibition is accomplished upon addition of 0.5 g/L and its polarization resistance and η_{EIS} are 28159.3 Ω cm^2 and 70.5%, respectively. It is noteworthy that the polarization resistances of 2.0 g/L LK and 2.0 g/L HCTZ are both smaller than that of blank solution, accompanied by a negative inhibiting efficiency of −28.2% and −66.1%, respectively. It is inferred that the degradation rate would be promoted by addition of LK and HCTZ with high concentrations. By comparison, it is evident that the EIS results are in good agreement with those of PDP.

The corrosion mechanism

Based on the analysis above, the addition of LK, NF and HCTZ antihypertensives with a proper concentration would be an effective approach to enhancing the corrosion resistance of AZ31 alloy in physiological environment. Hence, it is of great importance and necessity to in-depth understand the corrosion mechanism of AZ31 alloy influenced by these antihypertensives. Figure 12(a) depicts the schematic diagrams of corrosion mechanisms of AZ31 alloy in blank Hank's solution. Due to the high chemical activity of magnesium, the AZ31 alloy can be easily dissolved in physiological solution and a large amount of Mg^{2+} would be produced. The numerous Mg^{2+} dissociated around the surface of AZ31 alloy can react with OH^- existed in solution to form the $Mg(OH)_2$ film covering the alloy surface. Then calcium and phosphate ions would deposit on the surface of $Mg(OH)_2$ film to facilitate the nucleation and growth of hydroxyapatite[73], forming a Ca-P apatite layer eventually. In addition, some $Mg(OH)_2$ products would react with carbon dioxide dissolved in solution to form the magnesium carbonate($MgCO_3$). Therefore, the corrosion film on the AZ31 alloy is composed of $Mg(OH)_2$, hydroxyapatite and $MgCO_3$, among which the content of hydroxyapatite is relatively high. Although the formed corrosion film has a positive effect on the corrosion inhibition of AZ31 alloy, its effect is not desirable because of the porous and loose characteristic of film, which is caused by the massive hydrogen evolved from the alloy surface. Consequently, the AZ31 alloy has a poor anti-corrosion performance in blank Hank's solution.

After incorporating LK, NF and HCTZ antihypertensives into solutions, as illustrated in Fig. 12(b), the organic molecules in these antihypertensives can rapidly adsorb on the corrosion surface. The voids located on surface of the formed $Mg(OH)_2$ would be filled with these molecules, and the smooth and integrity of the film would be also strengthened. As a consequence, a compact and uniform hydroxyapatite layer may grow spontaneously on the surface of $Mg(OH)_2$ substrate. It can be also revealed from the EDS mapping and XPS results that the contents of Ca and P are all increased and the intensity of Ca 2p3/2 peaks is greatly enhanced upon addition of LK, NF and HCTZ antihypertensives. Compared with blank Hank's solution, the corrosion film formed on the surface of AZ31 alloy in the antihypertensives-containing solution has a stronger ability to hinder the magnesium ion from transporting onto the solution and inhibit the anodic dissolution of magnesium substrate underneath, thereby impeding the corrosion of AZ31 alloy and reducing its degradation rate. It should be noted that the higher concentrations of LK, NF and HCTZ antihypertensives may promote the corrosion of AZ31 alloy in Hank's solution. This adverse effect may be attributed to the fact that a severe agglomeration may occur among organic molecules at high concentrations. The agglomerated molecule clusters in solution could inevitably interact with the adsorbed molecules and result in the detachment of adsorbed molecules from the corrosion film. Once it happens, more fresh voids within the corrosion film would be exposed to the corrosive

solution, leading to the diminution of protection effect of the film, and thus the corrosion of AZ31 alloy would be increased. Apart from LK, NF and HCTZ, the other four antihypertensives such as ATEN, VLA, FUR and CAP show the negative inhibition effect on the corrosion of AZ31 alloy according to the electrochemical tests. It may be attributable to the fact that the ATEN, VLA, FUR and CAP molecules may react with Mg^{2+} to form the soluble complexes, eventually accelerating the dissolution of Magnesium. Therefore, they cannot function as effective surface modifiers to improve the corrosion resistance of AZ31 alloy but as the corrosion promoters to enhance the degradation of alloy.

Conclusions

In the present work, the effects of seven antihypertensives including LK, ATEN, NF, HCTZ, VLA, FUR and CAP on the degradation behavior of AZ31 magnesium alloy implants have been systematically investigated in simulated body fluid (Hank's solution). It is demonstrated that only LK, NF and HCTZ exhibit an inhibition effect on the corrosion of AZ31 alloy, and the highest inhibiting efficiency can be achieved upon addition of LK, NF and HCTZ with 0.5, 1.0 and 0.5 g/L, respectively. The electrochemical tests combined with the surface analysis reveal that the antihypertensives of LK, NF and HCTZ can promote the formation of uniform and compact hydroxyapatite layers with a high quantity on the surface of AZ31 alloy, leading to an enhanced protective effect of corrosion film, which can hinder the magnesium ion from transporting onto the solution and inhibit the anodic dissolution of magnesium substrate underneath. Hence, the corrosion of AZ31 alloy is greatly impeded and the degradation rate of alloy is remarkably reduced.

Data availability

All data included in this study are available upon request by contact with the corresponding author.

Received: 2 July 2025; Accepted: 16 October 2025
Published online: 20 November 2025

References

1. Poinern, G. E. J., Brundavanam, S. & Fawcett, D. Biomedical magnesium alloys: a review of material properties, surface modifications and potential as a biodegradable orthopaedic implant. *Am. J. Biomed. Eng.* **2** (6), 218–240 (2012).
2. Staiger, M. P., Pietak, A. M., Huadmai, J. & Dias, G. Magnesium and its alloys as orthopedic biomaterials: a review. *Biomaterials* **27** (9), 1728–1734 (2006).
3. Murugan, R. & Ramakrishna, S. Development of nanocomposites for bone grafting. *Compos. Sci. Technol.* **65** (15–16), 2385–2406 (2005).
4. Ye, X., Zion, T., Tang, G. & Song, G. Mechanical properties and phase transition of biomedical titanium alloy strips with initial quasi-single phase state under high-energy electropulses. *J. Mech. Behav. Biomed. Mater.* **42**, 100–115 (2015).
5. Ng, W., Chiu, K. & Cheng, F. Effect of pH on the in vitro corrosion rate of magnesium degradable implant material. *Mater. Sci. Eng. C.* **30** (6), 898–903 (2010).
6. Cui, L. Y. et al. In vitro corrosion resistance of layer-by-layer assembled polyacrylic acid multilayers induced Ca-P coating on magnesium alloy AZ31. *Bioact Mater.* **5** (1), 153–163 (2020).
7. Ali, A. et al. Hydrothermal deposition of high strength calcium phosphate coatings on magnesium alloy for biomedical applications. *Surf. Coat. Technol.* **357**, 716–727 (2019).
8. Chen, J., Song, Y., Shan, D. & Han, E. H. In situ growth process of Mg–Al hydrotalcite conversion film on AZ31 Mg alloy. *J. Mater. Sci. Technol.* **31** (4), 384–390 (2015).
9. Witte, F. et al. In vivo corrosion of four magnesium alloys and the associated bone response. *Biomaterials* **26** (17), 3557–3563 (2005).
10. Agarwal, S., Curtin, J., Duffy, B. & Jaiswal, S. Biodegradable magnesium alloys for orthopaedic applications: A review on corrosion, biocompatibility and surface modifications. *Mater. Sci. Eng. C.* **68**, 948–963 (2016).
11. Zeng, R., Dietzel, W., Witte, F., Hort, N. & Blawert, C. Progress and challenge for magnesium alloys as biomaterials. *Adv. Eng. Mater.* **10** (8), B3–B14 (2008).
12. Song, G. & Song, S. A possible biodegradable magnesium implant material. *Adv. Eng. Mater.* **9** (4), 298–302 (2007).
13. Rahyussalim, A. J., Supriadi, S., Kamal, A. F., Marsetio, A. F. & Pribadi, P. M. Magnesium-carbonate apatite metal composite: potential biodegradable material for orthopaedic implant. *AIP Conf. Proc.* **2092(1)**, 020021 (2019).
14. Walker, J., Shadanbaz, S., Woodfield, T. B., Staiger, M. P. & Dias, G. J. Magnesium biomaterials for orthopedic application: a review from a biological perspective. *J. Biomed. Mater. Res. B Appl. Biomater.* **102** (6), 1316–1331 (2014).
15. Song, M. S. et al. Recent advances in biodegradation controls over Mg alloys for bone fracture management: A review. *J. Mater. Sci. Technol.* **35** (4), 535–544 (2019).
16. Witte, F. The history of biodegradable magnesium implants: a review. *Acta Biomater.* **6** (5), 1680–1692 (2010).
17. Erisen, D. E. et al. Biosafety and biodegradation studies of AZ31B magnesium alloy carotid artery stent in vitro and in vivo. *J. Biomed. Mater. Res.* **12**, 1–10 (2021).
18. Razavi, M., Fathi, M., Savabi, O., Vashaee, D. & Tayebi, L. In vivo assessments of bioabsorbable AZ91 magnesium implants coated with nanostructured fluoridated hydroxyapatite by MAO/EPD technique for biomedical applications. *Mater. Sci. Eng. C.* **48**, 21–27 (2015).
19. Oshibe, N., Marukawa, E., Yoda, T. & Harada, H. Degradation and interaction with bone of magnesium alloy WE43 implants: A long-term follow-up in vivo rat tibia study. *J. Biomater. Appl.* **33** (9), 1157–1167 (2019).
20. Rad, H. R. B., Idris, M. H., Kadir, M. R. A. & Farahany, S. Microstructure analysis and corrosion behavior of biodegradable Mg-Ca implant alloys. *Mater. Des.* **33**, 88–97 (2012).
21. Zomorodian, A. et al. Corrosion resistance of a composite polymeric coating applied on biodegradable AZ31 magnesium alloy. *Acta Biomater.* **9** (10), 8660–8670 (2013).
22. Chen, X. et al. In vivo osseointegration of dental implants with an antimicrobial peptide coating. *J. Mater. Sci-Mater M.* **28**, 1–9 (2017).
23. Li, J., Chen, L., Zhang, X. & Guan, S. Enhancing biocompatibility and corrosion resistance of biodegradable Mg-Zn-Y-Nd alloy by Preparing PDA/HA coating for potential application of cardiovascular biomaterials. *Mater. Sci. Eng. C.* **109**, 110607 (2020).
24. Liu, D. et al. Influence of fine-grain and solid-solution strengthening on mechanical properties and in vitro degradation of WE43 alloy. *Biomed. Mater.* **9** (1), 015014 (2014).
25. Witte, F. et al. Degradable biomaterials based on magnesium corrosion. *Curr. Opin. Solid State Mater. Sci.* **12** (5–6), 63–72 (2008).

26. Xin, Y., Hu, T. & Chu, P. In vitro studies of biomedical magnesium alloys in a simulated physiological environment: a review. *Acta Biomater.* **7** (4), 1452–1459 (2011).
27. Song, Y., Han, E. H., Shan, D., Yim, C. D. & You, B. S. The effect of Zn concentration on the corrosion behavior of Mg–xZn alloys. *Corros. Sci.* **65**, 322–330 (2012).
28. Feyerabend, F. et al. Evaluation of short-term effects of rare Earth and other elements used in magnesium alloys on primary cells and cell lines. *Acta Biomater.* **6** (5), 1834–1842 (2010).
29. Sun, Z. L., Wataha, J. C. & Hanks, C. T. Effects of metal ions on osteoblast-like cell metabolism and differentiation. *J. Biomed. Mater. Res.* **34** (1), 29–37 (1997).
30. Witte, F., Ulrich, H., Rudert, M. & Willbold, E. Biodegradable magnesium scaffolds: part 1: appropriate inflammatory response. *J. Biomed. Mater. Res. A*. **81** (3), 748–756 (2007).
31. Yamamoto, A. & Hiromoto, S. Effect of inorganic salts, amino acids and proteins on the degradation of pure magnesium in vitro. *Mater. Sci. Eng. C*. **29** (5), 1559–1568 (2009).
32. Hoehlinger, M. et al. Influence of proteins on the corrosion behavior of a chitosan-bioactive glass coated magnesium alloy. *Mater. Sci. Eng. C*. **100**, 706–714 (2019).
33. Fang, H., Zhou, S., Qi, X., Tian, Y. & Wang, C. Hybrid plasma activation strategy for the Protein-Coated magnesium implants in orthopedic applications. *Adv. Mater. S Interfaces*. **9** (9), 2101724 (2022).
34. Li, L. Y. et al. Corrosion resistance of glucose-induced hydrothermal calcium phosphate coating on pure magnesium. *Appl. Surf. Sci.* **465**, 1066–1077 (2019).
35. Fan, X. L. et al. Corrosion resistance of an amino acid-bioinspired calcium phosphate coating on magnesium alloy AZ31. *J. Mater. Sci. Technol.* **49**, 224–235 (2020).
36. Zeng, R. C., Li, X. T., Li, S. Q., Zhang, F. & Han, E. H. In vitro degradation of pure Mg in response to glucose. *Sci. Rep.* **5** (1), 1–14 (2015).
37. Li, L. Y. et al. Microbial ingress and in vitro degradation enhanced by glucose on bioabsorbable Mg-Li-Ca alloy. *Bioact Mater.* **5** (4), 902–916 (2020).
38. Kirkland, N. T. & Waterman, J. Effect of amino acids and proteins on the in vitro performance of coated magnesium for biomedical applications. *Surf. Mod. Magnes Alloy Biomed. Appl.* **1**, 205–230 (2015).
39. Liu, C., Xin, Y., Tian, X. & Chu, P. K. Degradation susceptibility of surgical magnesium alloy in artificial biological fluid containing albumin. *J. Mater. Res.* **22** (7), 1806–1814 (2007).
40. Liu, C. et al. In vitro corrosion degradation behaviour of Mg–Ca alloy in the presence of albumin. *Corros. Sci.* **52** (10), 3341–3347 (2010).
41. Hornberger, H., Witte, F., Hort, N. & Mueller, W. D. Effect of fetal calf serum on the corrosion behaviour of magnesium alloys. *Mater. Sci. Eng. B*. **176** (20), 1746–1755 (2011).
42. Hou, R. et al. Adsorption of proteins on degradable magnesium-which factors are relevant? *ACS Appl. Mater. Interfaces*. **10** (49), 42175–42185 (2018).
43. Wang, Y. et al. In vitro degradation of pure magnesium-the effects of glucose and/or amino acid. *Materials* **10** (7), 725 (2017).
44. Li, L. Y. et al. In vitro corrosion of magnesium alloy AZ31-a synergetic influence of glucose and Tris. *Front. Mater. Sci.* **12**, 184–197 (2018).
45. Pokharel, D. B. et al. Effect of Glycine addition on the in-vitro corrosion behavior of AZ31 magnesium alloy in hank's solution. *J. Mater. Sci. Technol.* **81**, 97–107 (2021).
46. Gu, X., Zheng, Y. & Chen, L. Influence of artificial biological fluid composition on the Biocorrosion of potential orthopedic Mg-Ca, AZ31, AZ91 alloys. *Biomed. Mater.* **4** (6), 065011 (2009).
47. Cui, L. Y. et al. Vitro corrosion of Mg-Ca alloy-The influence of glucose content. *Front. Mater. Sci.* **11**, 284–295 (2017).
48. Bruneel, N. & Helsen, J. A. In vitro simulation of biocompatibility of Ti-Al-V. *J. Biomed. Mater. Res.* **22** (3), 203–214 (1988).
49. Cheng, X. & Roscoe, S. G. Corrosion behavior of titanium in the presence of calcium phosphate and serum proteins. *Biomaterials* **26** (35), 7350–7356 (2005).
50. Roach, P., Farrar, D. & Perry, C. C. Interpretation of protein adsorption: surface-induced conformational changes. *J. Am. Chem. Soc.* **127** (22), 8168–8173 (2005).
51. Mauser-Bunschoten, E., Fransen, D., Van De Putte, R. & Schutgens Co-morbidity in the ageing haemophilia patient: the down side of increased life expectancy. *Haemophilia* **15** (4), 853–863 (2009).
52. Chai, H., Ge, J., Li, L., Li, J. & Ye, Y. Hypertension is associated with osteoporosis: a case-control study in Chinese postmenopausal women. *BMC Musculoskelet. Disord*. **22**, 1–7 (2021).
53. Ilić, K., Obradović, N. & Vujasinović-Stupar, N. The relationship among hypertension, antihypertensive medications, and osteoporosis: a narrative review. *Calcif Tissue Int.* **92**, 217–227 (2013).
54. Schulz, M. et al. Medication adherence and persistence according to different antihypertensive drug classes: a retrospective cohort study of 255,500 patients. *Int. J. Cardiol.* **220**, 668–676 (2016).
55. Laurent, S. Antihypertensive drugs. *Pharmacol. Res.* **124**, 116–125 (2017).
56. Rizos, C. V. & Elisaf, M. S. Antihypertensive drugs and glucose metabolism. *World J. Cardiol.* **6** (7), 517–530 (2014).
57. Zhang, Y. et al. A study of degradation resistance and cytocompatibility of super-hydrophobic coating on magnesium. *Mater. Sci. Eng. B*. **78**, 405–412 (2017).
58. Cao, F., Shi, Z., Song, G. L., Liu, M. & Atrens, A. Corrosion behaviour in salt spray and in 3.5% NaCl solution saturated with Mg (OH) 2 of as-cast and solution heat-treated binary Mg-X alloys: X = Mn, Sn, Ca, Zn, Al, Zr, Si, Sr. *Corros. Sci.* **76**, 60–97 (2013).
59. Bahmani, A., Arthanari, S. & Shin, K. S. Improved corrosion resistant and strength of a magnesium alloy using multi-directional forging (MDF). *Int. J. Adv. Manuf. Technol.* **105**, 785–797 (2019).
60. Popov, B. N. *Corrosion Engineering: Principles and Solved Problems* 1st edn (Elsevier, Columbia, 2015).
61. Xue, F. et al. Effect of residual dissolved oxygen on the corrosion behavior of low carbon steel in 0.1 M $NaHCO_3$ solution. *J. Mater. Sci. Technol.* **34** (8), 1349–1358 (2018).
62. Umoren, S. A., Solomon, M. M., Madhankumar, A. & Obot, I. B. Exploration of natural polymers for use as green corrosion inhibitors for AZ31 magnesium alloy in saline environment. *Carbohydr. Polym.* **230**, 115466 (2020).
63. Li, H. et al. TiCN nanoparticle-induced corrosion Inhibition mechanisms of AZ91 alloy. *Corros. Sci.* **198**, 110109 (2022).
64. Feliu Jr, S. & Llorente, I. Corrosion product layers on magnesium alloys AZ31 and AZ61: surface chemistry and protective ability. *Appl. Surf. Sci.* **347**, 736–746 (2015).
65. Durham, J. W. III et al. Hydroxyapatite coating on PEEK implants: Biomechanical and histological study in a rabbit model. *Mater. Sci. Eng. C*. **68**, 723–731 (2016).
66. Cui, L. Y. et al. In vitro corrosion resistance of a layer-by-layer assembled DNA coating on magnesium alloy. *Appl. Surf. Sci.* **457**, 49–58 (2018).
67. Ong, J., Lucas, L., Raikar, G., Weimer, J. & Gregory, J. Surface characterization of ion-beam sputter-deposited Ca-P coatings after in vitro immersion. *Colloids Surf. Physicochem Eng. Asp*. **87** (2), 151–162 (1994).
68. Yan, W. et al. Vitro degradation of pure magnesium-the synergetic influences of glucose and albumin. *Bioact Mater.* **5** (2), 318–333 (2020).
69. Cuscó, R., Guiti´an, F., de Aza, S. & Artús, L. Differentiation between hydroxyapatite and β-tricalcium phosphate by means of μ-Raman spectroscopy. *J. Eur. Ceram. Soc.* **18** (9), 1301–1305 (1998).

70. Leonardo, H. E. R. N. A. N. D. E. Z. et al. Biomimetic hydroxyapatite (HAp) coatings on pure Mg and their physiological corrosion behavior. *Ceram. Int.* **48** (1), 1208–1222 (2022).
71. Krajewski, A. et al. Synthesis of carbonated hydroxyapatites: efficiency of the substitution and critical evaluation of analytical methods. *J. Mol. Struct.* **744**, 221–228 (2005).
72. Chow, L. C., Sun, L. & Hockey, B. Properties of nanostructured hydroxyapatite prepared by a spray drying technique. *J. Res. Natl. Inst. Stand. Technol.* **109**, 543 (2004).
73. Kokubo, T. Formation of biologically active bone-like apatite on metals and polymers by a biomimetic process. *Thermochim Acta*. **280**, 479–490 (1996).

Acknowledgements

The present study was sponsored by the National Key Research and Development Program of China under Grant no. 2021YFB3501001, the National Natural Science Foundation of China, People's Republic of China (NSFC) under Grant no. 51804197, and Natural Science Foundation of Inner Mongolia Autonomous Region of China under Grant no. 2024MS05048 and Science and Technology Cooperation Program and Science and Technology Cooperation Program of Shanghai Jiao Tong in Inner Mongolia Autonomous Region—Action Plan of Shanghai Jiao Tong University for "Revitalizing Inner Mongolia through Science and Technology".

Author contributions

G.X, M.F. and H.L.: Writing-original draft; Y.S and X.C.: Data curation; K.W. and H.Y: Writing—review & editing; G.W: Methodology; H.J.: Investigation.

Declarations

Competing interests

The authors declare no competing interests.

Additional information

Correspondence and requests for materials should be addressed to M.F., K.W. or G.W.